Salt enhanced solvent relaxation and particle surface area determination via rapid spin-lattice NMR

Laura N. Elliott [a,b,*], Richard A. Bourne [a,c], Ali Hassanpour [a], John L. Edwards [d], Stephen Sutcliffe [d], Timothy N. Hunter [a]

[a] School of Chemical and Process Engineering, University of Leeds, Leeds, LS2 9JT, United Kingdom
[b] Centre for Doctoral Training in Complex Particulate Products and Processes, University of Leeds, United Kingdom
[c] Institute of Process Research and Development, School of Chemistry, University of Leeds, United Kingdom
[d] Venator, Titanium House, Hanzard Drive, Wynyard Park, Stockton-on-Tees TS22 5FD, United Kingdom

ARTICLE INFO

ABSTRACT

This paper demonstrates the influence of surface charge chemistry on the application of nuclear magnetic relaxation measurements (NMR relaxometry) for the in situ determination of particle surface area, in the presence of high electrolyte concentration. Specifically, dispersions of titania, calcite and silica with and without 1 M KCl were investigated. The addition of salt, showed no significant change to relaxation measurements for titanium dioxide; however, a significant rate enhancement was observed for both calcite and silica systems. These differences were attributed to counterion layers forming as a result of the particles surface charge, leading to an increase in the relaxation rate of bound surface layer water. Further, changes appeared to be more pronounced in the silica systems, due to their larger charge. No enhancement was observed for titania, which was assumed to be due to the particles being at their isoelectric point, with no resulting counterion layer formation.

Solvent relaxation was further used to successfully determine the surface area of particles in a dispersion using a silica standard reference material, with results compared to Brunauer-Emmett-Teller (BET) and spherical equivalent estimations. Two different dispersions of titanium dioxide, of different crystal phases, were shown to have NMR surface area measurements in good agreement with BET. Thus showing the technique was able to measure changes in surface charge when surface chemistry remained relatively similar, due to the reference silica material also being an oxide. In contrast, the NMR technique appeared to overestimate the calcite surface areas in reference to BET, which was assumed to occur due to both better dispersion in the liquid state of nanocrystallites and potential ion enhancement from the solubility of the calcite. These results highlight the potential of this technique as a fast, non-destructive and non-invasive method for dispersion analysis, but also show the competition between surface area and surface chemistry interactions on measured relaxation rates.

© 2017 The Authors. Published by Elsevier B.V. This is an open access article under the CC BY license (http://creativecommons.org/licenses/by/4.0/).

1. Introduction

Particulate suspensions are present in numerous industries including pigments, cosmetics, pharmaceuticals and foods, and frequently, are at high concentrations [1]. Particle surface area is an important consideration, as an increase in the concentration of colloids in a dispersion results in a larger total surface area available, thus increasing the potential for surface reactions with the surrounding environment. The surface area of a particle is often determined for dry powders by Brunauer-Emmett-Teller (BET), whereby, nitrogen gas molecules physically adsorb onto a particle surface in layers [2,3]. Critically, BET is not capable of determining the total particle surface area for particles in solid-liquid (S-L) dispersions [4] and is considered to be somewhat time-consuming thus reducing its versatility, as some samples require extensive degas times, up to 24 h. Moreover, BET is dependent on the temperature and de-gas conditions used to obtain measurement reproducibility [5]. Mercury porosimetry and gravimetric analysis are alternative techniques for the measurement of surface area, although they also require dry powders [6]. It is well known that the drying of suspensions frequently leads to aggregation and agglomeration [7], resulting in measurements that are unreliable and misrepresentative of the particle surface area in a S-L dispersion [8].

Nuclear magnetic resonance (NMR) is commonly used for the identification of unknown compounds, while the use of proton relaxation rates allows the surface area to be obtained for any particle, of any size or shape [8]. Relaxation NMR (relaxometry) is a rapid non-invasive and non-destructive method to study the behaviour of liquids in porous and non-porous media [4,8]. It offers the potential for high speed data

acquisition, where relaxation measurements can be obtained between 5 and 15 min [4,8].

Relaxometry has previously been used to characterise many types of colloidal dispersions and interfacial phenomena, as recently reviewed by Cooper et al. [9]. Some examples include; polymers in aqueous solution and gels [10,11], polymer melts entanglement [12], polymer adsorption in the presence of electrolytes [13,14] and surfactant polymer interactions [15,16]. Furthermore, it has provided useful insight into competitive adsorption processes [17,18], and allows for a detailed understanding of the nature of the bound and free solvent sites in colloidal systems.

In 1987, Davis et al. [4], explored the use of solvent NMR to determine surface area and compared their findings to BET data [4]. Three different amorphous fumed silica powders were studied, these samples all had negligible internal porosity and therefore only a single exponential relaxation rate was observed, compared to a possible biexponential relaxation indicating water in pores [4]. Nearly three decades later, Fairhurst et al. [8], investigated dispersion and formulation behaviour of nanostructured carbon materials including graphene oxide, nanographite and porous graphene using NMR relaxometry [8], where particle aggregation and the influence of milling methods were also characterised [8]. Chen et al. have correlated relaxation NMR studies to determine the surface area of highly porous metal-organic frameworks to BET and Langmuir surface area measurements [19,20].

Relaxation NMR has also been used extensively to probe particle internal structure; for example, in geophysical well logging to estimate hydrocarbon-reservoir properties which include rock porosity, pore-size distribution, and permeability [21], while several studies have been conducted on the use of relaxation rates to examine porosity [22–25]. Literature has also shown that relaxation NMR measurements are useful to determine the specific surface area of porous cement materials [26], and study the effects of water reducing agents on sealing materials in cement [27].

Despite the number of previous studies, in wide research areas, there are still significant questions related to the application of NMR relaxometry for the measurement of colloidal surface areas, which has so far limited its wider use. In particular, is the influence of electrolyte conditions on the surface relaxation of solvent molecules, and whether bound counterion monolayers, enhance or reduce the relaxation rate. Flood et al. [13] studied the relative relaxation enhancement (R_{sp}) of four salts (NaCl, MgCl$_2$, CaCl$_2$ and LaCl$_3$) in water at a concentrations of 5 mM (below levels that led to aggregation excluding LaCl$_3$) with increasing concentrations of silica (0–10 wt%). They found the addition of salt led to an increase in the magnitude of R_{sp} which was dependent on the concentration and valency of the salt [13]. They suggested the addition of salt increases the silica-solvent affinity, in other words, there is an increase in the strength of binding of water at the silica surface as a function of ionic strength [13].

Although Flood et al. [13] were the first to conduct a valency and concentration study on the effects of salts to silica measured through NMR relaxation, there has been little progression within this area. Schwarz et al. [28] also carried out an NMR relaxation study on negatively charged sulphate-stabilised polystyrene latex nanoparticles (466 nm) in the presence of 0.25 M NaCl [28]. Consistent with Flood et al. [13] they reported a relaxation rate enhancement in the presence of salt, which they attributed to sodium ions forming a screening layer around the negatively charged latex particles [28]. It was assumed this screening caused an increase in the 'immobilised' water compared to the unscreened charges (where the term 'immobilised' referred to either increasing the amount of bound water to the particle surface, or, a reduction in the dynamics of the bound water) [28]. Additionally, Katika et al. [29] observed that chalk saturated with Mg-rich brines caused a shift in T$_2$ (spin-spin relaxation) to faster relaxation rates [29]. However, in their case, it was concluded that this result was due to precipitation within the pore space leading to an increase in the specific surface area [29].

While these few studies have indicated that electrolyte interactions generally result in an increase in relaxation rate, the underlying mechanism is still unclear. In addition, it is not known whether particle surface charge or magnitude may alter these effects. Importantly for application, there are also imperative questions as to what extent these effects may dominate or confound the use of these measurements for specific surface area analysis, greatly limiting the potential of NMR relaxation for on-line surface area measurements of concentrated slurries, for example [30].

To better understand these related phenomena, this paper presents NMR relaxation measurements in various systems, with changes in both particle surface area and interfacial chemistry. Titanium dioxide, calcium carbonate and silica were selected, due to their likely differences in particle charge at neutral pH [31–33]. Additionally, their fine and cohesive nature, resulting in broad size distributions are representative of many commonly encountered industrial suspensions [34]. Systems with and without 1 M KCl were characterised, where the high salt concentration was thought to considerably enhance any potential ion effects, but also induce particle aggregation (and thus lower total surface area).

2. NMR surface area theory

A dispersion constituting a single liquid and single particulate material is simplified to contain two liquid domains that have different relaxation rates [25,26], where a monolayer coverage of fluid on the particle surface is assumed. The first domain being the bulk liquid (R_b) which is far away from the particle surface and the second the bound solvent (R_s), which is the liquid molecules on the surface of the particle [4]. The liquid bound at the particle surface has a relaxation time orders of magnitude shorter than the comparative bulk (2–3 s), as their motion becomes anisotropic and restricted, thus enhancing the relaxation rate [8,17]. However, only a single average relaxation time is observed due to the fast interchange of the bulk and bound solvent [8,17]. The average relaxation rate (R_{av}) is weighted by the quantity of fluid in each domain, whereby the domains are additive as shown by Eq. (1) [8]. Here, R_{av}, R_b and R_s (ms^{-1}) are various solvent relaxation rates, detailed above, ψ_p is the particle to liquid volume ratio (dimensionless), S (m^2/g) is the total surface area per unit weight, L (m) is the surface layer thickness of the bound liquid, while ρ_p is the bulk particle density (g/m^3).

$$R_{av} = \psi_p\, S\, L\, \rho_p\, (R_s - R_b) + R_b \tag{1}$$

The use of a standard reference material of a known surface area, allows a constant to be defined K_a, which for a given interface, can in principle be obtained for any material. This parameter is a surface specific relaxation constant (g/m^2/ms), shown by Eq. (2), where K_a is dependent on both particle type, associated surface chemistry and solvent [8]. While, this dependency has limited the techniques use in some systems, nonetheless, it still provides a simple and rapid method to extract important information regarding changes in wetted surface area. Similar theory has previously been denoted for the online surface area measurements of concentrated slurries [30].

$$k_a = L\, \rho_b\, (R_s - R_b) \tag{2}$$

The particles' specific surface area for a given particle system is calculated by substituting Eq. (2) into Eq. (1) and rearranging, as shown by Eq. (3) [8]. Here, R_{sp} is known as the specific relaxation enhancement (Eq. (4)) which is a dimensionless number [9,17].

$$S = \frac{R_{sp} R_b}{K_a \psi_p} \tag{3}$$

$$R_{sp} = \frac{R_{av}}{R_b} - 1 \tag{4}$$

Hence, the total surface area of particles in a suspension is calculated from the gradient of the R_{sp} plot as a function of particle volume ratio (ψ_p) [8]. It is well accepted this theory holds true for a given particle-solvent system when:

- There is a fast exchange between the bulk and bound solvent and the NMR relaxation times are markedly different, where the bulk relaxation time is longer.
- A material with a high surface area should have a shorter relaxation time, as more fluid is bound to the surface.
- The particle systems are well dispersed and do not sediment during the relaxation measurement.
- Relaxation NMR is also dependent on temperature and frequency conditions and must, therefore, be kept constant throughout the measurement.

However, the authors propose a reduction of Eq. (2) to allow for the surface area determination of multiple particle systems from the use of a single reference interface, as shown in Eq. (5). Here, K_a is the unknown materials specific surface relaxation constant (g/m^2/ms), K_c (g/m^2/ms) is the calculated material specific relaxation constant of a standard reference material of known surface area. Here, ρ_b is the bulk particle density (g/m^3) of the material of interest, and ρ_{bc} is the bulk particle density (g/m^3) of the standard reference material.

$$K_a = \frac{K_c \rho_b}{\rho_{bc}} \tag{5}$$

The replacement of Eq. (5) into Eq. (3), allows the determination of a particle's surface area. This theory requires that the following assumptions are met;

- The solvent remains constant and only a monolayer coverage of the bound solvent is assumed, thus both R_b and L are unchanged.
- Similar surface chemistries and conditions are required, and thus there must be negligible change in R_s.

In reality, there are many potential factors that may affect R_s for different particle systems, or for the same particle systems in different surface environments. For example, the adsorption of surfactants and polymers has a big effect on R_s relaxation which is not captured by this equation. Other factors that can influence the rate of relaxation of surface bound water include, pH [35], paramagnetic species [9] and the presence of ^{27}Al [36], for example. For, silica, pH extremes were found to enhance relaxation rates as observed by van der Beek et al. [35], whereas the relaxation rate for water was independent of pH. This enhancement for silica is due to proton exchange occurring at the particle surface between water and surface hydroxyl groups. Further, the dissolution of particles can result in relaxation rate enhancements, which for silica, this may occur above pH 12, and is a result of paramagnetic impurities entering into the bulk solution [35]. However, this paper looks to explore the effect of two related phenomena; the influence of particle charge and high electrolyte conditions, and secondly the influence of surface chemistry differences from similar oxides and carbonate minerals.

3. Materials and methods

3.1. Materials

An initial NMR calibration was made using Ludox AS-40, 40 wt% suspension standard (Sigma-Aldrich) which is denoted as *silica^a* throughout this paper. Silica^a has a particle size 20–24 nm, and a specific surface area of 135 m^2/g, as quoted by the supplier [37]. Silica^a was received suspended in distilled H$_2$O and an ammonium stabilising counterion. Dispersions were purified using an ion exchange resin Amberlite

MB-150 (MP Biomedicals) to remove any residual electrolyte effects from the standard. Angstrom Sphere silica microspheres (Fiber Optic Center) were used and this silica is represented as *silica^b* from herein. Silica^b was supplied as a powder, where microspheres were stated as ~100 nm from the manufacturer. The density of both silica 'a' and 'b' was taken to be 2.2 g/cm^3 [38]. Pre-calcined (anatase) titanium dioxide (supplied by Venator Materials PLC) was also used, denoted *TiO$_2^g$*, as this material is known by the manufacturer to have a high surface area, due to reduced crystallinity of the anatase phase. The density of titanium dioxide, anatase, was taken as 3.79 g/cm^3 [39]. Further measurements were conducted on another titanium dioxide (99.5% purity), obtained from Sigma-Aldrich and used without purification, denoted as *TiO$_2^b$*. TiO$_2^b$ was previously used in the synthesis of Ti(SO$_4$)O nanocatalyst by Gardy et al. [40] where the precursor was fully characterised in terms of crystal structure, particle size and BET surface area.

Calcium carbonate (in the calcite polymorphic form), calcite Omyacarb *2AZ* (Omya) was also used in this study, due to its incorporation into many consumer products. The density of calcite was taken as 2.71 g/cm^3, supplied by the manufacturer. Stock acid and base solutions were prepared to vary the pH of suspensions; hydrochloric acid (Sigma-Aldrich), reagent grade, 37% was used to decrease the pH and potassium hydroxide pellets (Sigma-Aldrich) were used to increase the pH. Pure potassium chloride salt (Sigma-Aldrich) was used throughout to alter salt concentrations. NMR resonant frequency measurements were performed to calibrate the frequency, using a copper sulphate solution as received (Xigo Nanotools). Ethanol absolute was purchased from Fisher Scientific and used as received for transmission electron microscopy sample preparation.

3.2. Methods

Prior to any analysis or characterisation, suspensions were dispersed using an ultrasonic bath (Clifton Sonic) for 30 min. Samples were further dispersed using an ultrasonic probe, Sonic Dismembrator (Fisher Scientific), at 30% amplitude for 1 min. All particle-salt measurements were also dispersed using this procedure and then left to mix for 24 h on a carousel, to ensure the KCl had dissolved and allow time for any particle coagulation to occur.

3.2.1. Particle size and morphology

The particle size, morphology and surface structures were studied for TiO$_2^a$ using a scanning electron microscope (SEM) SU8230 (Hitachi). Prior to SEM analysis, the TiO$_2^a$ powder was placed onto an SEM stub and excess powder was removed by spraying with compressed air. TiO$_2^a$ samples were coated before SEM analysis with a carbon coating of 10 nm using a Q150TE sputter coater (Quorum). SEM images were also obtained for calcite using EVO MA15 (Carl Zeiss). Calcite samples were prepared similarly to TiO$_2^a$, although, an iridium coating of 10 nm thickness was used. The particle size of two silica samples silica^a and silica^b were investigated using bright field transmission electron microscopy (TEM) FEI Tecnai F20-G2 FEGTEM operating at 200 kV. The silica^a suspension as supplied was pipetted directly onto a copper grid coated with holey carbon film and left to dry, and Silica^b was first suspended in ethanol with vigorous shaking before pipetting onto the grid. When conducting imaging, standard alignments were performed and samples were imaged across a wide magnification range, with numerous areas acquired. Thus, the images selected are representative of the samples analysed.

Particle size distributions were measured for calcite and TiO$_2^a$, using a Mastersizer 2000 (Malvern), with a standard operating procedure (SOP) of 10 runs, and a measurement taken after every 10 s, these 10 runs were then averaged to produce a single distribution. Silica^b particle size distributions were obtained using a Zetasizer Nano ZS (Malvern) with the instrument set to three measurements, each consisting of 15 cycles. The three measurements were then averaged to produce a single particle size distribution for silica^b with and without 1 M KCl.

The Mastersizer 2000 (Malvern) could not be used for TiO_2^a and calcite salt-particle size measurements, due to high shear in the cell, thought to break up coagulated particles. Instead, a Camsizer P4 dynamic image analyser (Retsch Technology), was employed to study the changes in particle size in the presence of the KCl electrolyte. Calcite and TiO_2^a suspensions were first prepared both at 1 vol% in ultrapure water and 1 M KCl using a stock solution, and suspensions were dispersed as previously stated. The Camsizer ultrasonic bath was switched off during these particle size measurements to reduce the shear in the cell and avoid breakage of any coagulated particles. A stock 10 mM KCl solution was used as the dispersant fluid in the attached Camsizer ultrasonic bath, and the circulation pump was set to 100%. The Camsizer SOP was set to three measurements which was then averaged to produce a single distribution, with each run stopping after 80,000 images were analysed.

3.2.2. Settling measurements

A 12 channel Lumisizer Dispersion Analyser (LUM GmbH) was employed to investigate the sedimentation rate of the dispersions, and to further support particle coagulation and changes in particle size distributions. Calcite and TiO_2^a dispersions (1 vol%) were prepared in ultrapure water and with 0.1 and 1 M KCl stock solutions. These suspensions were all dispersed as stated in Section 3.2 and then pipetted into a 10 mL polyamide sample cell PA 110-135XX (LUM GmbH). Settling test were carried out at 25 °C, using a transmission wavelength of 865 nm. The measurement SOP was set to 300 RPM, measuring 90 profiles with 10 s intervals. Each dispersion was run in duplicate and the results were averaged.

3.2.3. Surface charge

A Zetasizer Nano ZS (Malvern) was used to measure the zetapotentials of calcite, TiO_2^a and silica[b]. Prior to analysis, a stock KCl solution was prepared at 0.1 mM in ultrapure deionised water. TiO_2^a, calcite and silica[b] dispersions were prepared at a concentration of 1000 ppm each with the stock KCl electrolyte (0.1 mM) and samples were dispersed as per Section 3.2. Further to this, stock base (KOH) and acid (HCl) solutions were prepared at 0.01, 0.1 and 1 M, to increase and decrease the pH of particle dispersions, respectively. For each surface charge measurement, one dispersion was made to vary with acid and another with base. All dispersions were kept mixing with a magnetic stirrer for approximately 10 min after altering the pH. The pH of suspensions were then measured using HI-208 Bench top pH meter (Hanna Instruments), before pipetting into DTS1070 folded capillary cells (Malvern). The zetasizer SOP was set for 3 measurements with a maximum of 100 profiles for each, the measurement automatically terminated when 10 stable profiles were sequentially collated. A total of 6 measurements were collected at each pH point on the zetapoential curve and averaged data was recorded with standard deviations.

3.2.4. Crystal structure

The x-ray powder diffraction patterns for TiO_2^a was obtained to investigate the nature of the crystalline phase, using a D8 X-ray Diffractometer (Bruker) and CuKα radiation source. The TiO_2^a sample was scanned from 2θ angle 10° to 70° with a step size 0.0495° at 35 s per step.

3.2.5. Surface characterisation

The Brunauer–Emmett–Teller (BET) surface area and pore size measurements were obtained by the nitrogen adsorption-desorption method at 77.3 K using a TriStar 3000 (Micromeritics) surface analyser. TiO_2^a samples were degassed to remove any moisture and surface absorbed gases by using a vacuum oven at 120 °C for 24 h under a vacuum of 10 mmHg. The calcite samples were degassed under N_2 for 4 h at 300 °C, and atmospheric pressure. Silica[b] was degassed under vacuum oven at 100 °C for 17 h overnight under a vacuum of 10 mmHg. The N_2 adsorption isotherms were used to calculate the BET parameters

for both TiO_2^a and calcite; and desorption isotherms were used to calculate the average pore size by the Barrett-Joyner-Halenda (BJH) method.

3.2.6. Relaxation NMR measurements

Silica[a] was used as a reference material. Prior to measuring the T_1 relaxation rates, dispersions were made in ultrapure water at 30, 20, 10 and 1 wt%. These suspensions were left to stir with a magnetic stirrer bar for 24 h with an ion exchange resin, as stated in Section 3.1, the ion exchange resin was then removed by Buchner filtration. Silica[b] dispersions were prepared at 1.1, 2.4, 3.3 and 5.0 wt% in ultrapure water, and 1.0, 2.4, 3.3 and 5.0 wt% with 1 M KCl. TiO_2^a dispersions were prepared at 10, 15, 20 and 25 wt% in ultrapure water and 10, 20 and 30 wt% in 1 M KCl. TiO_2^b dispersions were used at 5 and 10 wt% in ultrapure water. Similarly, calcite suspensions were prepared at 15, 20, 35, 40, 45 and 50 wt% without salt and 44, 37 and 13 wt% with 1 M KCl. All suspensions were dispersed according to the protocol in Section 3.2 before T_1 relaxation measurements were obtained.

All relaxation measurements were acquired using a spin-lattice relaxation (T_1) time for H nuclei and were performed on an Acorn Area (Xigo Nanotools), 13 MHz desktop NMR spectrometer. Relaxation measurements were completed for all suspensions, by removal of 0.5 mL aliquots, which were pipetted into NMR tubes. Former to any relaxation measurements the resonance frequency was measured using a copper sulphate solution standard (described in Section 3.1). A 90°-pulse length of 5.67 μs and 180°-pulse length of 11.33 μs was utilised for all measurements.

A T_1 experiment was planned according to the following procedure; an inversion-recovery sequence was measured with 11 points, averaging 4 scans with a recycle delay of 5 times the anticipated T_1 value. The 11 points on the magnetization vs time curve were planned based on 2^n, where n equals, the time spacing T (ms). Measurements along the curve started at a time T (ms) of one thousandths of the recycle delay, increasing with 2^n until reaching the final 11th point. The anticipated T_1 value was initially approximated for each new particle dispersion or bulk liquid measurement, until the expected T_1 was within 20% of the final T_1 measurement. Once the anticipated T_1 was within this range, three repeat measurements were performed and an average obtained. For example, an anticipated T_1 value of 1000 ms would give a recycled delay of 5000 ms and a planned inversion recovery sequence would range from T 5 (ms) to 5120 (ms).

4. Results and discussion

4.1. Particle characterisation

Scanning electron microscopy (SEM) images were obtained for TiO_2^a and calcite as shown in Fig. 1. SEM images of calcite (Fig. 1a) display the faceted nature of the particles, which is important to note as particle size measurements assume sphericity. In some cases, nanocrystallites were found to be agglomerated onto larger particles (Fig. 1a inset). Fig. 1b (inset) demonstrates the highly aggregated nature of TiO_2^a, with individual crystallites in the order of ~20–100 nm. TiO_2^a crystallites are fused together to form larger particles and a representative cluster is presented in Fig. 1b. These TiO_2^a clusters ranged in Feret diameter between 1 and 3 μm.

The zetapotential recorded in background electrolyte is shown for TiO_2^a, calcite and silica in Fig. 2. The pH_{iep} for TiO_2^a was ~6 and in good agreement with previous literature [31]. Fig. 2 also shows calcite to be positively charged, but unstable, fluctuating around 0–10 mV almost across the entire pH range studied. It is also noted that the partial solubility of calcite leads to a bi carbonate ion formation, which caused an increase in measured neutral pH to pH 8–9 (still within the region of positive charge). These values are also consistent with literature, where Somasundaran et al. [32] reported a pH_{iep} for calcite at approximately pH 10.5, with a positive trend and characteristic S-shape curve from pH 7.0–10.5 [32]. Silica[b] was negatively charged across the entire
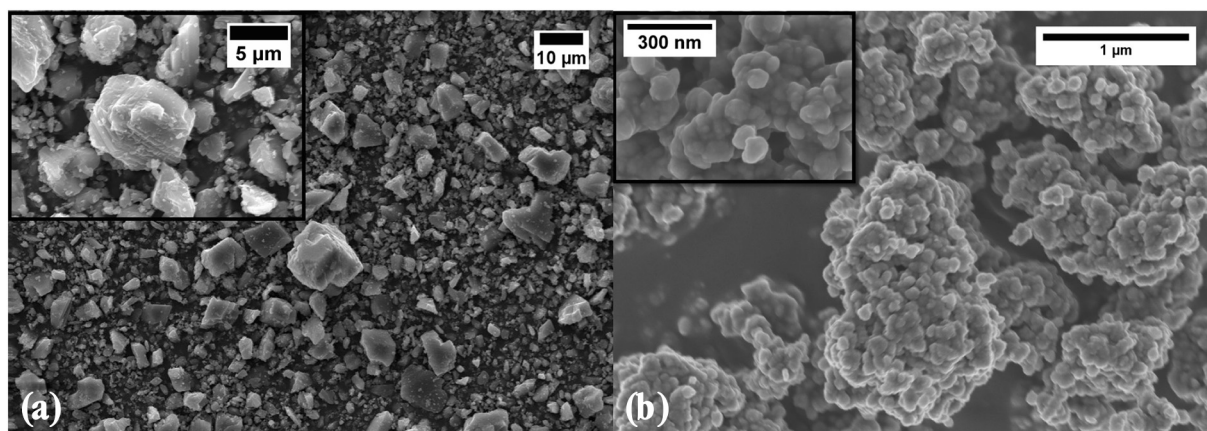
Fig. 1. SEM images of (a) calcite, scale bar 10 μm and inset scale bar 5 μm. SEM images of (b) titanium dioxide (TiO$_2^a$) scale bar 1 μm and inset scale bar 300 nm.

pH range studied, approaching the pH$_{iep}$ towards pH 2, and in concurrence with silica literature values ranging from pH$_{iep}$ 1–2 [33].

Fig. 3, shows the particle size distribution (PSD) for TiO$_2^a$ and calcite, where, it is observed TiO$_2^a$ has a monomodal distribution, with a measured D$_{50}$ of 1.63 μm, which is in accordance with the observed clusters from SEM analysis (Fig. 1). Calcite was found to have a slightly broader bimodal distribution and a D$_{50}$ of 3.24 μm.

The effect of 1 M KCl on the PSD for TiO$_2^a$ and calcite, measured with the Camsizer, is presented in Fig. 4. As this data relies on image collection rather than Mie theory, the limit of the detection is ~1 μm, thus the distributions in Fig. 4 are not directly comparative to those in Fig. 3. However, it is evident in Fig. 4(a) that the addition of 1 M KCl to TiO$_2^a$ shows little change in the PSD, with only a small increase in volume % (3%) is observed around 10 μm, suggesting perhaps some slight coagulation of smaller particles. More apparent, is the increase in particle size for calcite in the presence of 1 M KCl, demonstrated by the growth of the peak height for particles of ~100 μm in size. It is noted that there is evidence for calcite aggregation without salt, with a small but distinct aggregate peak also at ~100 μm, which was not observed from the Mastersizer data in Fig. 3. This difference is most likely due to a reduction in the level of the dispersion technique inside the measurement cell of the Camsizer (Fig. 4) compared to the Mastersizer (Fig. 3), this suggests for calcite the camsizer does not disperse as well. Bux et al. [1] observed a similar phenomenon in titania PSD, dependent on dispersion mechanism. Although calcite shows a net positive surface charge

(Fig. 2), this has a relatively small magnitude, and therefore it can be expected that some level of aggregation may take place regardless, although it is clear the majority of calcite particles in 0 M KCl are well dispersed.

The change in silica^b PSD in the presence of 1 M KCl and without electrolyte was also investigated, as observed in Fig. 5. The particle-water dispersion has a narrow monomodal size distribution with a D$_{5o}$ of 110 nm, which increases to a D$_{5o}$ of 171 nm in 1 M KCl and a much broader distribution, thus illustrating the coagulation of silica^b in the presence of the 1 M KCl electrolyte.

Suspension settling rates under centrifugation were also used to elucidate changes in particle aggregation for TiO$_2^a$ and calcite, with the addition of KCl electrolyte. Here, Fig. 6, represents changes in dispersion height measured over time for titania and calcite systems in the Lumisizer. Average settling rates were approximated from the linear regime of the settling profiles in Fig. 6 (represented by the dashed lines). It can be observed from Fig. 6 that there is little to no change in the settling time for TiO$_2^a$ when in the presence of either 0.1 M or 1 M KCl, demonstrating that the titaina is similarly aggregated regardless of solvent conditions. In contrast, both the 0.1 M and 1.0 M KCl calcite dispersions settled to a compacted bed in approximately 100 s, whereas the 0 M KCl calcite dispersion reached an analogous bed height in 900 s. While such an order of magnitude increase in settling rate, correlates to a 3–4 times increase in particle size (if related to the Stokes terminal settling equation) in reality this comparison is only qualitative and probably underestimates the aggregation in salt significantly. The reason is that, at 1 vol% all dispersions are likely within hindered settling
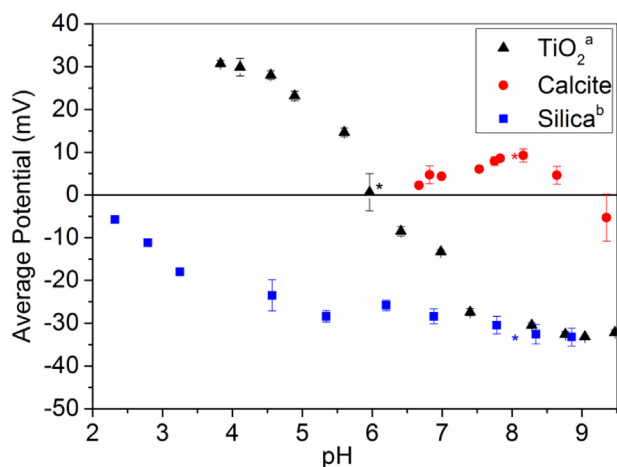

Fig. 2. Zetapotentials for TiO$_2^a$ (triangle), calcite (circle), and silica^b (square) in background electrolyte (1 × 10^{-4} M KCl). The pH of each dispersion for NMR measurements are indicated by coloured asterisks (*). (For interpretation of the references to colour in this figure legend, the reader is referred to the web version of this article.)
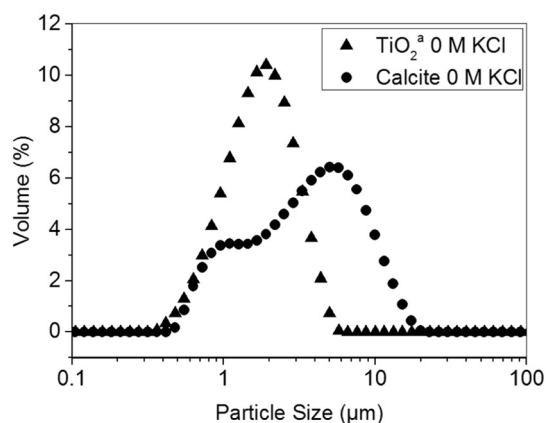

Fig. 3. Particle size distributions from laser diffraction for sonicated calcite (circle), and TiO$_2^a$ (triangle) dispersions without salt.
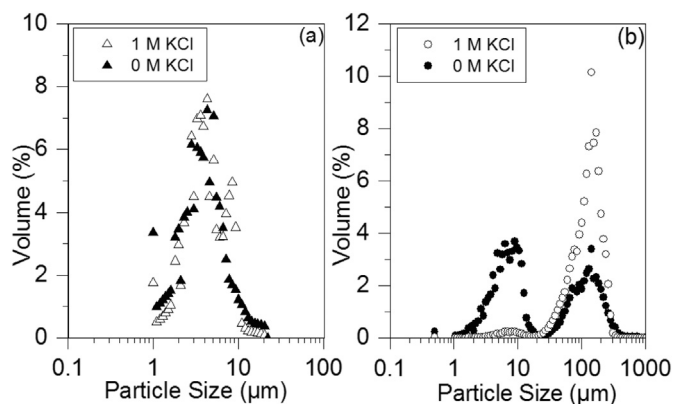
Fig. 4. Particle size distribution from dynamic image analysis (a) TiO_2^a (triangle), and (b) calcite (circle), both in the presence of 0 M KCl (closed) and 1 M KCl (open).

zone conditions, where coagulation may significantly enhance hindered settling effects [41].

4.2. NMR relaxation calibration

Ludox silica particles (silica[a]) were used for the NMR calibration, which had a known surface area, quoted from the manufacturer as 135 m²/g and 20–24 nm in size [37]. The quoted surface area is in agreement with the calculated surface area (124 m²/g), if a spherical shape is assumed, with an average particle size of 22 nm. Transmission electron microscopy (TEM) images (Fig. S1, Supplementary information), show the silica[a] to be spheroidal, but with slightly irregular shapes and thus the larger quoted surface area is consistent with their morphologies.

Fig. 7 presents the measured T_1 relaxation rates of these silica dispersions, for various concentrations <20 vol%. An increase in the concentration of silica[a] was found to cause a decrease in the average relaxation time (as shown in Fig. 7(a)). This result is expected, since the liquid bound at the particle surface relaxes faster than the comparative bulk, and a higher concentration of particles leads to a larger total surface area and hence an increase in the fraction bound water. Thus, overall the relaxation time shortens as particle concentration is increased.

Fig. 7 displays the T_1 relaxation rate against the product of increasing particle volume ratio and known surface area of silica[a]. Eq. (3) indicates that this relationship should yield a straight line trend, with a gradient proportional to K_a (the specific surface relaxation constant) which is dependent on both solvent and solid [4,42]. The K_a value extracted from the average slope for silica[a] was 4.05×10^{-5} g/m²/ms. A relaxation time of 2652.1 ms was measured for bulk H_2O, (no solids present),
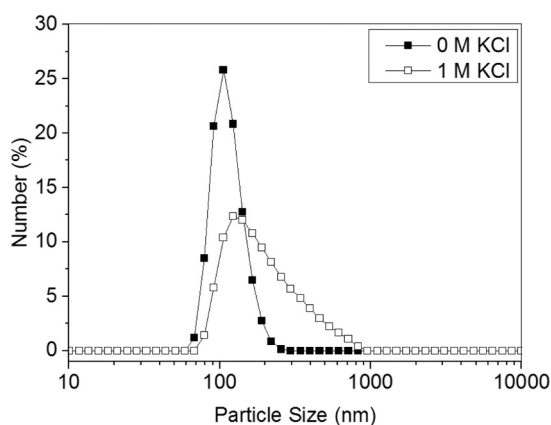

Fig. 5. Particle size distribution for silica[b] particles after 24 h of mixing on carousel at 1 wt %, in the presence of 0 M KCl (closed) and 1 M KCl (open).

equating to a relaxation rate of 0.377×10^{-3} ms^{-1}. Further, theory states the y-intercept of the relaxation rate versus the product of the particle volume ratio and surface area, should yield $1/R_b$, where R_b is the relaxation rate of the bulk liquid [4,42]. Fig. 7(b), has a y-intercept of 0.389×10^{-3} ms^{-1}, and comparing this result to the bulk relaxation rate measured for H_2O, suggests the error on this calibration measurement is around 3%. Glaves et al. [42] state that relaxation measurements are reproducible within approximately 1% and to study low surface areas, the difference between R_b and R_s must be significant compared to the accuracy of the measurement [42]. From herein, the specific surface relaxation constant determined for silica[a] (4.05×10^{-5} g/m²/ms), denoted K_c in Eq. (5), was used to calculate the unknown specific surface relaxation constants K_a (Eq. (5)) for TiO_2^a, calcite and silica[b].

4.3. Enhancement of specific solvent relaxation in high electrolyte conditions

Relaxation NMR could prove to be a useful measurement when determining surface areas in the presence of surface modifiers, for example dispersive electrolytes or polymers. As previously discussed within the introduction, relaxation measurements can become significantly more complicated at interpreting in the presence of electrolytes, due to counterion effects. Here, 1 M KCl electrolyte was used to observe changes in relaxation, as a result of particle coagulation and competing counterion effects.

The NMR relaxation time was measured with increasing particle concentration for TiO_2^a, calcite and silica[b], and the relative relaxation enhancement R_{sp} was calculated using Eq. (4). Figs. 8–10 show the relative relaxation enhancement (R_{sp}) as a function of particle to volume ratio (Ψ_p) for TiO_2^a, calcite and silica[b] respectively. It is expected from NMR relaxation theory that an increase in particle concentration results in a decrease in the relaxation time, equating to an increase in the R_{sp}, which is observed for Figs. 8–10. As aforementioned, this is because water at the particle surface has a faster relaxation time than water further away in the bulk, as the particle concentration increases, more surface becomes available, and thus a faster relaxation time is observed.

The relaxation time was measured for bulk 1 M KCl (R_b) without any solids present, which gave a value of 2907 ms (shown in Fig. 8(a)). The R_b of bulk water was measured as approximately 2652 ms (shown in Figs. 7(a) and 8(a)). Comparing the R_b of the salt solution to R_b of pure water gives a relative relaxation enhancement (R_{sp}) of 0.1 for the solution only, similar to relative enhancements previously observed in the literature [13]. This enhancement of 0.1 R_{sp} was enough to warrant a calibration of R_b to equal that of the salt solution rather than pure water, for the calculated R_{sp} for all particle-salt dispersions. Hence, Figs. 8–10 show the R_{sp} of dispersions going through the origin of the R_{sp} versus Ψ_p plots, for both system types with and without salt. Table 1 summarises the measured K_a values (from the water systems), as well as the gradient values of the R_{sp}/Ψ_p relationships with and without 1 M KCl. The enhancement ratio in electrolyte conditions (comparing both R_{sp}/Ψ_p gradients) is also shown. It should be noted that Fig. 8(c) shows the relaxation NMR data for the TiO_2^b dispersions in water only, (this data will be discussed in Section 4.4, in relation to surface area measurements).

It is evident that the electrolyte has a negligible effect on the relaxation times measured in TiO_2^a, compared to the water dispersions, as shown by Fig. 8. Here, the gradient of the R_{sp}/Ψ_p values with and without electrolyte has a calculated enhancement ratio of 1.05. As previously demonstrated by particle size and settling measurements, TiO_2^a remains highly aggregated irrespective of solvent conditions. Thus, there is assumed to be no significant change in surface area for the high salt system, and it is possible to probe relaxation purely based on counterion effects. Therefore, it would appear these results are counter to enhancements in silica and latex systems found previously [13,28]. The TiO_2^a particle dispersions for the NMR measurements had a recorded pH of 6.1 and the zetapotential measurements shown in Fig. 2 clearly indicated the TiO_2^a was around its isoelectric point (IEP). Hence, there should be
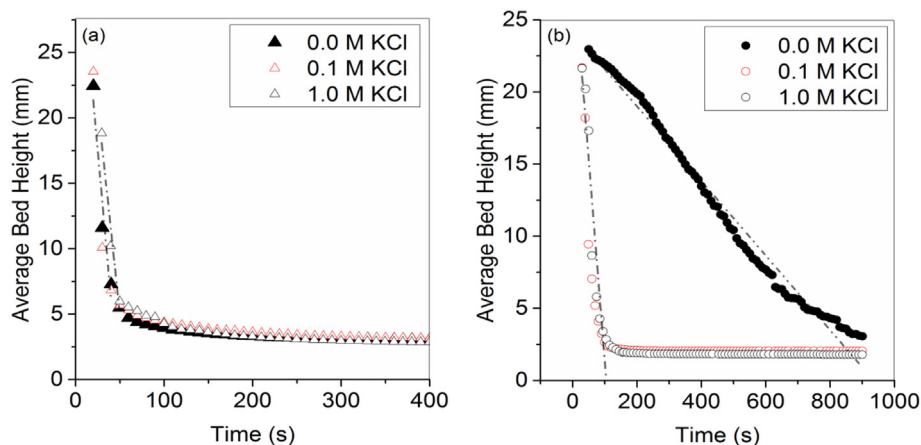
Fig. 6. Average Lumisizer interface versus time measurements at 300 rpm for 1 vol% dispersions undergoing sedimentation, of TiO_2^a (a) and calcite (b) in 0 M (black closed), 0.1 M (red open) and 1 M (black open) KCl. Dashed lines indicate the linear rates. (For interpretation of the references to colour in this figure legend, the reader is referred to the web version of this article.)

no significant counterion layer around the particles, suggesting interaction between the particle surface and attracted ions may be critical to relaxation measurements, rather than simply electrolyte concentration.

Particle size, zetapotential and settling measurements have shown both calcite and silica[b] to be coagulated in the presence of 1 M KCl; hence, a decrease in surface area would be expected, leading to a decrease in the R_{sp}/Ψ_p gradient. In contrast to this, both calcite and silica[b] particle-salt dispersions were found to have a considerable increase in R_{sp} compared to particle-water dispersions (Figs. 9 and 10 respectively). The R_{sp}/Ψ_p enhancement ratio is given Table 1. For calcite, this ratio was found to be almost twice that of the corresponding particle-water gradient, while silica[b] it was over three times greater.

The pH of the calcite dispersions during the NMR experiments was measured to be at ~ pH 8, and the zetapotential measurements (Fig. 2) illustrate that dispersions will be positively charged, as the calcite IEP is approximately pH 9. Therefore, a screening counterion layer of negatively charged chlorine ions, will form around the positively charged calcite surface. For silica[b], dispersions were also used with a pH of ~8. Thus, conversely, the silica will be strongly negatively charged (Fig. 2) and a positive screening layer of potassium ions will form around the surface. The authors propose the increase in the R_{sp} observed for calcite and silica (Figs. 9 and 10) is due to this counterion effect, resulting in an increased relaxation rate for the bound water (R_b). This stipulation is further supported by the absence of the increase in R_{sp} for titania-salt dispersions (Fig. 8), which is at the IEP, as discussed. It is interestingly noted also, that as high salt conditions were used, the diffuse electric double layer is assumed to be negligible. Nevertheless, as surface relaxation is assumed to occur from monolayer molecules, it is likely the inner Helmholtz plane only influences behaviour. While similar

relative enhancements for particle-salt dispersions have been reported in the literature and such specific ion effect have been proposed [13,28], the influence of particle zetapotential charge and magnitude, and related influence of agglomeration have not previously been observed.

Additionally, the authors suggest the increase in the magnitude of the R_{sp}/Ψ_p gradient for silica[b] compared to calcite may be due to the increased magnitude of the surface charge of the silica (Fig. 2). However, this conclusion is difficult to state for certain, due to the confounding impact of aggregation, which would be expected to reduce the total surface area and thus the R_{sp}. This is an area of ongoing investigation. Indeed, enhancement from the counterion effect alone may be expected to be even greater than measured in these systems, as the overall relaxation rate will be partially reduced from the lower particle surface area in high salt conditions.

4.4. Comparison of BET and NMR surface area determination

The relative relaxation enhancement (R_{sp}) for particle-water dispersions (Figs. 8–10) were used to determine the specific surface area of the two different titania samples, calcite and silica[b] (using Eq. (3)) and compared to BET measurements in Table 2. The R_{sp} of particle-salt dispersions were not used to calculate surface area due to the competing counterion effects outlined.

The specific surface relaxation constant previously determined for silica[a] (4.05×10^{-5} g/m^2/ms), denoted K_c in Eq. (5), and was used to calculate K_a for silica[b], TiO_2^a, TiO_2^b and calcite and using respective particle densities. Table 2 also shows a calculated surface area comparison, assuming spherical particle shapes, and the previously recorded particle
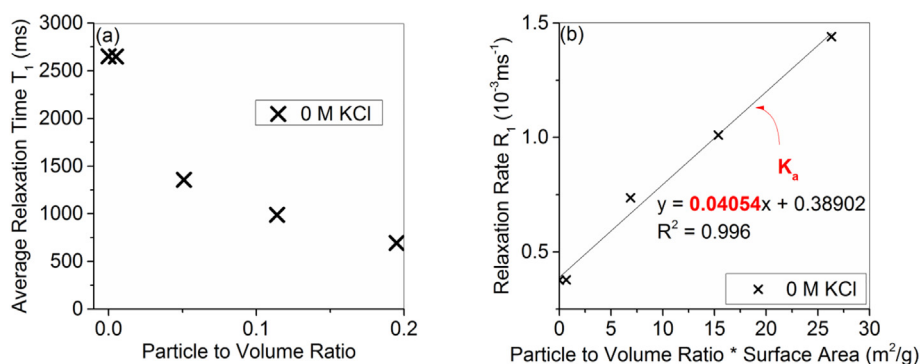
Fig. 7. Calibration measurements for silica[a] (Ludox standard) particles (a) relaxation time vs particle to volume ratio and (b) average relaxation rates with the product of increasing particle volume ratio and known silica[a] surface area (137 m^2/g).
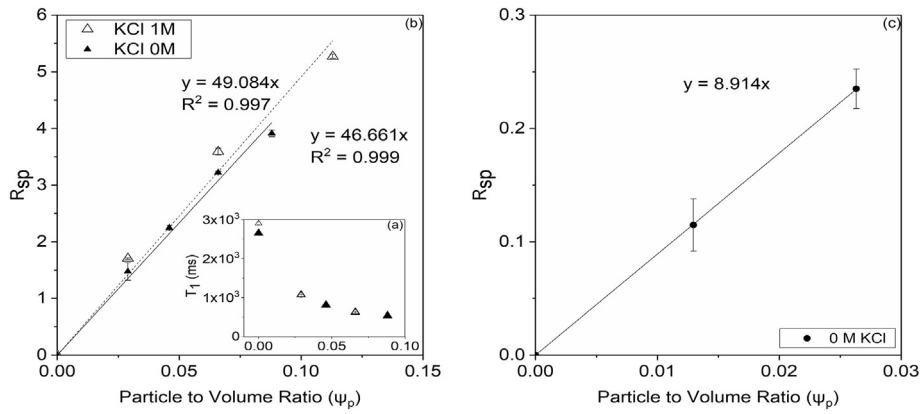
Fig. 8. (a) shows average relaxation times (T_1) for TiO_2^a with increasing particle concentration (φ_p) with and without 1 M KCl. (b) Relative relaxation rate enhancement (R_{sp}) for TiO_2^a with increasing particle concentration in 0 M KCl (closed triangle) and 1 M KCl (open triangle). (c) TiO_2^b relative relaxation rate enhancement in 0 M KCl.

D_{50} values. The BET nitrogen adsorption-desorption isotherms are shown for TiO_2^a, calcite and silica^b, in Figs. S2–S4 (Supplementary information), alongside the pore size distributions and total pore volumes.

For silica^b (Table 2) the BET surface area was ~12 m^2/g compared to the NMR surface area ~30 m^2/g, the smaller surface area obtained from the BET is most likely due to the agglomerated nature of silica^b, thus leading to several particle contact points where nitrogen adsorption cannot occur, hence causing the underestimation of the true surface area of silica^b in a dispersion. However, silica^b NMR surface area is in good agreement with the calculated spherical surface area (Table 2, ~28 m^2/g), where Fig. S1 (Supplementary information), shows the TEM images of silica^b is monodispersed and uniformly spherical. Here, the value of using relaxation NMR is clearly highlighted, where BET otherwise failed, for determining surface area accurately for small colloidal particles where the surface chemistry remains unchanged compared to the reference material.

Comparison of the TiO_2^a specific surface area data highlighted in Table 2, shows that there is excellent agreement between the NMR SA (~253 m^2/g) and the BET SA (~263 m^2/g). This result is significant, as it provides evidence of the ability to measure particle SA for solid-liquid dispersions, in this case, where there is a change in surface potential yet surface chemistry remains similar as both the systems studied are oxides. It is important to note that the spherical estimates for the SA calculation of TiO_2^a is misleading, giving a surface area of ~1 m^2/g (Table 2). The very large SA of TiO_2^a would equate more to the

nanocrystallites (20–100 nm), observed from SEM analysis (Fig. 1) and not the measured D_{50}, which is agglomerated TiO_2^a.

Further to these results, TiO_2^b NMR SA (47 m^2/g) is also in good agreement with the BET SA (49 m^2/g), obtained from Gardy et al. [40], as shown in Table 2. It appears both TiO_2 samples are within 4% of the corresponding BET measurements, which is significant, as sample conditioning requires a fraction of the time, without reducing the reproducibility and accuracy of the NMR measurements. Hence, it has been shown that a single calibration k_a can be used for different particle systems of similar chemistries, despite the fact that the surface charges were considerably different between the titania and silica^a standard. These results are consistent with findings from van der Beek et al. [35], who investigated the influence of pH on the relaxation rate of silica and water dispersions. Despite changes in the surface charge of silica across a broad pH range the relaxation rate remained largely unchanged, at least in low electrolyte conditions. However, they did observe differences under extreme pH conditions, indicating relaxation enhancements as a result of, fast proton exchange and partial dissolution of silica.

Uncertainty in the phase purity and crystallinity of the TiO_2^a used was speculated, due to the very high surface area results obtained. For this reason, XRD analysis was conducted on the commercial sample (Fig. S5, Supplementary information). Commercial titania of high surface areas are typically around 50 m^2/g (Degussa p-25) [43], however, Wei et al. [44] reported the synthesises of high purity phase pure anatase TiO_2 with a BET surface area of 186 m^2/g [44]. The XRD patterns for TiO_2^a was measured and indexed using JCPDS-ICDD and confirmed the anatase phase (04-013-5313, TiO_2) [45]. Line broadening can be observed in the XRD spectra and is most likely due to the poor crystallinity.
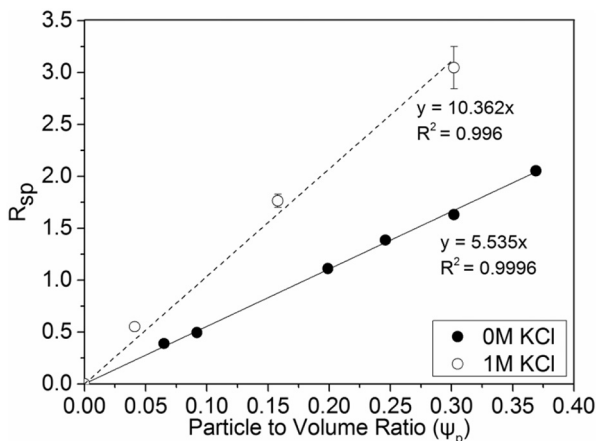
Fig. 9. Relative relaxation rate enhancement (R_{sp}) for calcite with increasing particle concentration in 0 M KCl (closed circle) and 1 M KCl (open circle).
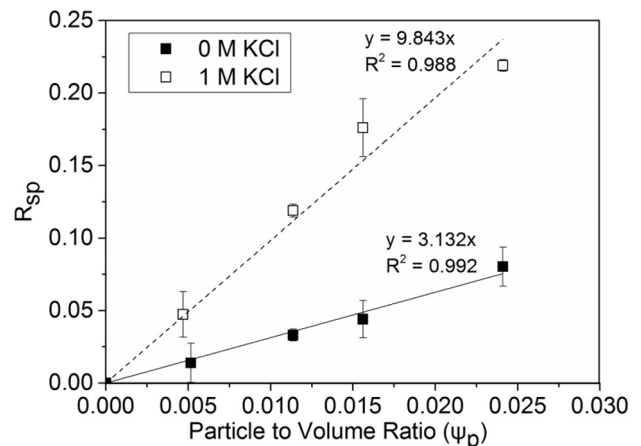
Fig. 10. Relative relaxation rate enhancement (R_{sp}) for 100 nm silica^b with increasing particle concentration in 0 M KCl (closed) and 1 M KCl (open).

Table 1

Summary of NMR constants, gradients of the R_{sp}/Ψ_p plots with and without KCl, where the ratio of this change in gradient has been calculated*.

Material	Density (g/cm³)	K_a specific surface relaxation constant (g/m²/ms)	Gradient 0 M KCl $\frac{R_{sp}}{\Psi_p}$	Gradient 1 M KCl $\frac{R_{sp}}{\Psi_p}$	Ratio*
Silica[a]	2.2	4.05×10^{-5}	n/a	n/a	n/a
TiO₂[a]	3.79	6.98×10^{-5}	46.661	49.084	1.05
TiO₂[b]	3.9	7.18×10^{-5}	8.917	n/a	n/a
Calcite	2.71	4.99×10^{-5}	5.535	10.362	1.87
Silica[b]	2.2	4.05×10^{-5}	3.132	9.843	3.14

Additionally, literature has shown BET trends for amorphous TiO_2 typically have higher surface areas than crystalline counterparts, with values usually >250 m²/g [46].

The calculation of calcite surface area using relaxation NMR (Table 2, ~42 m²/g) was not found to be in good agreement with the BET results (~2 m²/g), which leads to the uncertainty of the true surface area for either measurements. A recent study by Agnihotri et al. [47] showed the influence of surface modifiers on the structure of precipitated calcium carbonate [47]. Here, they recorded Linwood carbonate (having a 97% composition wt% of calcium carbonate) to have a BET surface area of 1.9 m²/g for a D_{50} particle size of 6 μm [47]. This result is of a similar value for a comparable D_{50}, thus giving confidence in the BET surface area results obtained for calcite in this study. Further, the calculated calcite surface area (Table 2 ~0.6 m²/g) using the calcite D_{50} equivalent spherical diameter is of a similar magnitude to the BET SA (~2 m²/g). The calculated value for calcite marginally underestimates the SA compared to BET, likely from calcite being more faceted (Fig. 1). Therefore, there is some uncertainty in the much larger surface area estimate obtained for calcite using relaxation NMR.

However, it should not necessarily be expected that the surface area of the two measurement techniques will always give the same values, as the BET measurement requires a dry powder, and in contrast, relaxometry measures the wetted particle surface area. SEM images of calcite (Fig. 1), show agglomeration of nanocrystallites onto the surface of larger particles (~250 nm). If these nanocrystallites are better dispersed during the NMR measurement, these smaller fines would dominate the measurement. As the water bound to the surface relaxes faster than the bulk, this would lead to a larger surface area observed for the NMR measurement compared to the BET. Although, N_2 can diffuse into primary particles of aggregates during the BET measurement, bound nanocrystallites onto the primary particles' surface could lead to a reduction in the surface area measured by BET.

The aforementioned study by Agnihotri et al. [47] reported surface areas for precipitated calcium carbonate of 17 m²/g obtained without the presence of surface modifiers, which increased to values between 40 and 60 m²/g in the presence of a surface modifier Dispex [47]. Here, it is clearly shown the better dispersed the calcium carbonate, the larger the surface area (although, results were all obtained from BET measurements). Hence, the difference in the surface area results

could be merely down to calcite nanocrystallites being well dispersed during the NMR measurements, however, these would need to be in the order of ~50 nm to equate for a spherical equivalent surface area of 42 m²/g.

Adding further complexity to the system, the solubility of the calcite could also lead to some degree of re-precipitation back onto the calcite surface, which again may increase the surface area detected for the NMR compared to the BET. Potential re-precipitation mechanisms would be consistent with previous explanations for enhanced surface areas calculated from NMR by Katika et al. [29] in brine enriched chalk rocks.

A more plausible explanation to the large NMR surface area might be due to the partial solubility of calcium carbonate in water (0.013 g/L at 25 °C) [48], which may perhaps lead to an increase in the relaxation rate due to an increase in electrolyte concentration, leading to enhancements from counterion effects previously discussed. Thus, overall leading to an over estimation of the NMR surface area for calcite. More generally, the interfacial chemistry of the calcite is not similar enough to silica to allow for this reference material to be used, and thus the assumptions of Eq. (5) are no longer valid as the water bound at the particle interface ($\mathbf{R_s}$) is significantly changed.

5. Conclusions

Electrolyte effects on relaxation NMR were investigated for a range of particle systems of differing particle charge. TiO_2^a was found to be unaffected by solvent conditions, remaining highly aggregated, and a negligible effect on the relaxation rate enhancement (R_{sp}) was observed under electrolyte conditions. It was concluded that due to the neutral particle charge during relaxation measurements no significant counterion screening layer was formed, and hence no additional relaxation enhancement was observed. In complete contrast, both calcite and silica[b], showed substantial enhancements in the R_{sp} in the presence of the KCl electrolyte. This was attributed to a counterion effect inducing a screening layer around both calcite and silica (although oppositely charged), which increased the R_{sp} as a result of the enhancement in the particle-solvent affinity. Additionally, an increase in the magnitude of the R_{sp}/Ψ_p gradient for silica[b] compared to calcite was noted. It was suggested this could be caused by the increased magnitude of the surface charge for silica[b], although further work is required for a more comprehensive understanding of this phenomena.

Relaxation NMR was used to successfully calculate the surface area of two titanium dioxide samples for highly concentrated suspensions, where there was excellent agreement between the NMR and BET surface area measurements. Further, relaxation NMR was also used effectively to calculate the surface area of silica[b], where BET otherwise failed. However, although the successes of solvent relaxation to calculate specific surface area were demonstrated, there was uncertainty in measurements of calcite surface area. The surface area calculated for calcite by NMR was far larger than by BET, which the authors propose is most likely due to both better dispersion of nanocrystallites in the liquid state, and partial solubility of calcite in water. Importantly, these results highlight that while the use solvent relaxation to study particle surface area offers faster experimental times and greater compatibility compared to conventional techniques, counterion effects make the interpretation of NMR relaxation rates significantly more complicated than theory suggests in many cases.

Table 2

Comparison of the calculated NMR surface area (SA), BET and calculated spherical surface area obtained from the particle size distribution for silica[b], TiO₂[a], TiO₂[b] and calcite. *TiO₂[b] BET surface area measurements were performed by Gardy et al. [40] alongside **TEM particle size analysis.

Material	BET surface area (m²/g)	Calculated spherical surface area [based on D_{50} (μm)] (m²/g)	Calculated NMR surface area (m²/g)
Silica[a]	n/a	124 [0.022]	n/a
Silica[b]	11.74 ± 0.05	27.3 [0.110]	29.9 ± 1.4
TiO₂[a]	262.64 ± 1.95	0.971 [1.631]	252.8 ± 6.4
TiO₂[b]	48.64*	69.9 [0.022]**	47.0 ± 0.1
Calcite	2.38 ± 0.01	0.648 [3.418]	41.8 ± 0.3

Data statement

The article metadata is available in the University of Leeds repository, https://doi.org/10.5518/352, entitled, Laura Elliott (2018): Salt enhanced solvent relaxation during rapid spin-lattice NMR data set University of Leeds. [Dataset]. Article metadata is available under a Creative Commons Attribution licence (CC-BY).

Acknowledgements

Appendix A. Supplementary data

Supplementary data to this article can be found online at https://doi.org/10.1016/j.powtec.2018.04.050.

References

[1] J. Bux, J. Peakall, S. Biggs, T.N. Hunter, In situ characterisation of a concentrated colloidal titanium dioxide settling suspension and associated bed development: application of an acoustic backscatter system, Powder Technol. 284 (2015) 530–540.

[2] S. Lowell, J.E. Shields, Adsorption isotherms, Powder Surface Area and Porosity, Springer, Netherlands, Dordrecht 1991, pp. 11–13.

[3] K.S.W. Sing, 6th International Conference on Surface and Colloid Science, The use of gas adsorption for the characterization of porous solids, Colloids and Surfaces 38 (1989) 113–124.

[4] P.J. Davis, D.P. Gallegos, D.M. Smith, Rapid surface area determination via NMR spin-lattice relaxation measurements, Powder Technol. 53 (1987) 39–47.

[5] K. Sing, The use of nitrogen adsorption for the characterisation of porous materials, Colloids Surf. A Physicochem. Eng. Asp. 187–188 (2001) 3–9.

[6] S. Lowell, J.E. Shields, M.A. Thomas, M. Thommes, Other Surface Area Methods, Characterization of Porous Solids and Powders: Surface Area, Pore Size and Density, Springer, Netherlands, Dordrecht, 2004 82–93.

[7] P. Bowen, C. Carry, From powders to sintered pieces: forming, transformations and sintering of nanostructured ceramic oxides, Powder Technol. 128 (2002) 248–255.

[8] D. Fairhurst, T. Cosgrove, S.W. Prescott, Relaxation NMR as a tool to study the dispersion and formulation behavior of nanostructured carbon materials, Magn. Reson. Chem. 54 (2016) 521–526.

[9] C.L. Cooper, T. Cosgrove, J.S. van Duijneveldt, M. Murray, S.W. Prescott, The use of solvent relaxation NMR to study colloidal suspensions, Soft Matter 9 (2013) 7211–7228.

[10] Y.E. Shapiro, Structure and dynamics of hydrogels and organogels: an NMR spectroscopy approach, Prog. Polym. Sci. 36 (2011) 1184–1253.

[11] J. Spěváček, NMR investigations of phase transition in aqueous polymer solutions and gels, Curr. Opin. Colloid Interface Sci. 14 (2009) 184–191.

[12] T. Cosgrove, M.J. Turner, P.C. Griffiths, J. Hollingshurst, M.J. Shenton, J.A. Semlyen, Self-diffusion and spin-spin relaxation in blends of linear and cyclic polydimethylsiloxane melts, Polymer 37 (1996) 1535–1540.

[13] C. Flood, T. Cosgrove, I. Howell, P. Revell, Effects of electrolytes on adsorbed polymer layers: poly(ethylene oxide)—silica system, Langmuir 22 (2006) 6923–6930.

[14] C. Flood, T. Cosgrove, Y. Espidel, I. Howell, P. Revell, Sodium polyacrylate adsorption onto anionic and cationic silica in the presence of salts, Langmuir 23 (2007) 6191–6197.

[15] E. Pettersson, D. Topgaard, P. Stilbs, O. Söderman, Surfactant/nonionic polymer interaction. A NMR diffusometry and NMR electrophoretic investigation, Langmuir 20 (2004) 1138–1143.

[16] Z. Gao, R.E. Wasylishen, J.C.T. Kwak, NMR studies in surfactant and polymer-surfactant systems: micelle formation of sodium ω-phenyldecanoate and interaction with poly(ethylene oxide), J. Colloid Interface Sci. 137 (1990) 137–146.

[17] C.L. Cooper, T. Cosgrove, J.S. van Duijneveldt, M. Murray, S.W. Prescott, Competition between polymers for adsorption on silica: a solvent relaxation NMR and small-angle neutron scattering study, Langmuir 29 (2013) 12670–12678.

[18] A. Nelson, K.S. Jack, T. Cosgrove, D. Kozak, NMR solvent relaxation in studies of multicomponent polymer adsorption, Langmuir 18 (2002) 2750–2755.

[19] J.J. Chen, X. Kong, K. Sumida, M.A. Manumpil, J.R. Long, J.A. Reimer, Ex situ NMR relaxometry of metal–organic frameworks for rapid surface-area screening, Angew. Chem. 125 (2013) 12265–12268.

[20] J.J. Chen, J.A. Mason, E.D. Bloch, D. Gygi, J.R. Long, J.A. Reimer, NMR relaxation and exchange in metal–organic frameworks for surface area screening, Microporous Mesoporous Mater. 205 (2015) 65–69.

[21] E. Grunewald, R. Knight, A laboratory study of NMR relaxation times and pore coupling in heterogeneous media, Geophysics 74 (2009) E215–E221.

[22] C. Terenzi, C. Casieri, F. De Luca, R. Quaresima, G. Quarta, V. Tudisca, Firing-induced microstructural properties of quasi-diamagnetic carbonate-based porous ceramics: a 1H NMR relaxation correlation study, Appl. Magn. Reson. 46 (2015) 1159–1178.

[23] X. Li, Y. Li, C. Chen, D. Zhao, X. Wang, L. Zhao, H. Shi, G. Ma, Z. Su, Pore size analysis from low field NMR spin–spin relaxation measurements of porous microspheres, J. Porous. Mater. 22 (2015) 11–20.

[24] D.P. Gallegos, D.M. Smith, C.J. Brinker, An NMR technique for the analysis of pore structure: application to mesopores and micropores, J. Colloid Interface Sci. 124 (1988) 186–198.

[25] D.P. Gallegos, K. Munn, D.M. Smith, D.L. Stermer, A NMR technique for the analysis of pore structure: application to materials with well-defined pore structure, J. Colloid Interface Sci. 119 (1987) 127–140.

[26] F. Barberon, J.P. Korb, D. Petit, V. Morin, E. Bermejo, What is the surface specific area of porous cement-based material? A nuclear magnetic relaxation dispersion approach, Magn. Reson. Imaging 21 (2003) 355–357.

[27] X. Li, B. Lin, C. Zhai, G. Ni, Z. Li, Relaxation study of cement based grouting material using nuclear magnetic resonance, Int. J. Min. Sci. Technol. 22 (2012) 821–824.

[28] B. Schwarz, M. Schönhoff, A 1H NMR relaxation study of hydration water in polyelectrolyte mono and multilayers adsorbed to colloidal particles, Colloids Surf. A Physicochem. Eng. Asp., 198–200 (2002) 293–304.

[29] K. Katika, M. Adassi, M.M. Alam, I.L. Fabricius, Changes in specific surface as observed by nmr, caused by saturation of chalk with porewater bearing divalent ions, Diffusion Fundamentals 22 (2014) 1–14.

[30] S.B. Thoma, D.M. Smith, J. Boughton, R. Davies, On-line surface area measurement of concentrated slurries using low field spin-lattice relaxation NMR, Part. Part. Syst. Charact. 10 (1993) 246–251.

[31] J. Gustafsson, P. Mikkola, M. Jokinen, J.B. Rosenholm, The influence of pH and NaCl on the zeta potential and rheology of anatase dispersions, Colloids Surf. A Physicochem. Eng. Asp. 175 (2000) 349–359.

[32] P. Somasundaran, J.O. Amankonah, K.P. Ananthapadmabhan, Mineral—solution equilibria in sparingly soluble mineral systems, Colloids and Surfaces 15 (1985) 309–333.

[33] P. Wilhelm, D. Stephan, On-line tracking of the coating of nanoscaled silica with titania nanoparticles via zeta-potential measurements, J. Colloid Interface Sci. 293 (2006) 88–92.

[34] A. Weir, P. Westerhoff, L. Fabricius, K. Hristovski, N. von Goetz, Titanium dioxide nanoparticles in food and personal care products, Environ. Sci. Technol. 46 (2012) 2242–2250.

[35] G.P. Van der Beek, M.A.C. Stuart, T. Cosgrove, Polymer adsorption and desorption studies via proton NMR relaxation of the solvent, Langmuir 7 (1991) 327–334.

[36] C.L. Cooper, T. Cosgrove, J.S. van Duijneveldt, M. Murray, S.W. Prescott, Colloidal particles in competition for stabilizer: a solvent relaxation NMR study of polymer adsorption and desorption, Langmuir 28 (2012) 16588–16595.

[37] Sigma-Aldrich Ludox Silica AS-40 Data Sheet, http://www.sigmaaldrich.com/catalog/product/aldrich/420840?lang=en&region=GB (22/05/2017).

[38] M. Hosokawa, K. Nogi, M. Naito, T. Yokoyama, Nanoparticle Technology Handbook, Elsevier Science, 2007.

[39] J.H. Braun, A. Baidins, R.E. Marganski, TiO2 pigment technology: a review, Prog. Org. Coat. 20 (1992) 105–138.

[40] J. Gardy, A. Hassanpour, X. Lai, M.H. Ahmed, Synthesis of Ti(SO$_4$)O solid acid nanocatalyst and its application for biodiesel production from used cooking oil, Appl. Catal. A Gen. 527 (2016) 81–95.

[41] M. Johnson, J. Peakall, M. Fairweather, S. Biggs, D. Harbottle, T.N. Hunter, Characterization of multiple hindered settling regimes in aggregated mineral suspensions, Ind. Eng. Chem. Res. 55 (2016) 9983–9993.

[42] C.L. Glaves, P.J. Davis, D.M. Smith, Surface area determination via NMR: fluid and frequency effects, Powder Technol. 54 (1988) 261–269.

[43] V.A. Yasir, P.N. MohanDas, K.K.M. Yusuff, Preparation of high surface area TiO$_2$ (anatase) by thermal hydrolysis of titanyl sulphate solution, Int. J. Inorg. Mater. 3 (2001) 593–596.

[44] X. Wei, G. Zhu, J. Fang, J. Chen, Synthesis, characterization, and photocatalysis of well-dispersible phase-pure anatase TiO$_2$ nanoparticles, International Journal of Photoenergy 2013 (2013) 6.

[45] L. Aldon, P. Kubiak, A. Picard, J.C. Jumas, J. Olivier-Fourcade, Size particle effects on lithium insertion into Sn-doped TiO$_2$ anatase, Chem. Mater. 18 (2006) 1401–1406.

[46] T. Froschl, U. Hormann, P. Kubiak, G. Kucerova, M. Pfanzelt, C.K. Weiss, R.J. Behm, N. Husing, U. Kaiser, K. Landfester, M. Wohlfahrt-Mehrens, High surface area crystalline titanium dioxide: potential and limits in electrochemical energy storage and catalysis, Chem. Soc. Rev. 41 (2012) 5313–5360.

[47] R. Agnihotri, S.K. Mahuli, S.S. Chauk, L.-S. Fan, Influence of surface modifiers on the structure of precipitated calcium carbonate, Ind. Eng. Chem. Res. 38 (1999) 2283–2291.

[48] G.F. Aylward, Tristan, SI Chemical Data Book, 4th ed. John Wiley & Sons, Australia, 2008.